Optical Materials 35 (2013) 1173–1178

Contents lists available at SciVerse ScienceDirect

Optical Materials

journal homepage: www.elsevier.com/locate/optmat

Spectroscopic study of red-light-emitting centers in $K_2Al_2B_2O_7$: Fe single crystals

I.N. Ogorodnikov [a,*], V.A. Pustovarov [a], S.A. Yakovlev [a], L.I. Isaenko [b]

[a] Ural Federal University, 19, Mira Street, 620002 Yekaterinburg, Russia
[b] Institute of Geology and Mineralogy of SB RAS, 43, Russkaya Street, 630058 Novosibirsk, Russia

ARTICLE INFO

Article history:
Received 21 November 2012
Received in revised form 7 January 2013
Accepted 7 January 2013
Available online 19 February 2013

Keywords:
Luminescence
Optical spectra
Temperature dependence
Impurity defects
KABO

ABSTRACT

We report on spectroscopic study of red-light-emitting centers in $K_2Al_2B_2O_7$ (KABO) single crystals containing ca. 2 ppm of Fe^{3+}. Owing to the low Fe^{3+}-concentration, KABO does not show noticeable absorption due to Fe^{3+} *d*–*d*-transitions in the visible spectral region, but it exhibits the charge-transfer (CT) UV-absorption bands O–Fe at 4.7, 5.7 and 6.5 eV. The red photoluminescence at 1.675 eV (FWHM = 0.173 eV) is due to intracenter $^4T_1$ (^4G) → $^6A_1$ (^6S) transitions in Fe^{3+} ions. Because of partial overlapping of the fundamental absorption edge of the crystal, where mobile excitons are created, and a broad CT absorption band at 6.5 eV, the most intensive red emission occurs at 7 K upon excitation in the excitonic energy region. The presence of two nonequivalent Al_2O_7 clusters in KABO lattice provides two different types of red-light-emitting centers in the form of Fe^{3+} ion occupied the Al^{3+} tetrahedral site. Superposition of their luminescence bands determines both the spectrum and temperature dependence of red emission in KABO at T = 7–80 K: two bands with the ratio of intensities of ca. 2:1 are 20 meV-shifted relative to each other; two-stage thermal quenching obeys the Mott law with E_T = 9 and 20 meV.

1. Introduction

Potassium aluminum borate, $K_2Al_2B_2O_7$ (KABO), is a comparatively novel optical material developed to operate in a broad spectral range from 180 to 3600 nm [1–3]. The KABO crystals are non hygroscopic, mechanically strong, and have excellent nonlinear optical properties [4]. They are prospective to use in high-power light sources of ultraviolet (UV) and vacuum ultraviolet (VUV) coherent radiation, generated as the fourth harmonic (266 nm) or sum frequencies (up to 193 nm) from the fundamental radiation of Nd^{3+} lasers [5–8].

KABO belongs to a trigonal crystallographic system (space group symmetry P321), its unit cell contains 39 atoms (Z = 3) [1–3,5,9], and the lattice parameters are $a = b = 0.85669(8)$ nm, $c = 0.8467(1)$ nm [3]. From literature it is known [3] that KABO crystal lattice consists of a three-dimensional network composed of corner sharing BO_3 triangles and Al_2O_7 units. Because of the crystal symmetry there are two different independent configurations of Al_2O_7 units with the ratio of their amounts of 2:1. In all cases, the Al^{3+} ion is four-coordinated by oxygen atoms, and the deviation from ideal tetrahedral geometry is small [3].

Growing KABO crystals from ordinary pure raw materials leads to the introduction of uncontrolled iron impurities [1]. Fe^{3+} defects have been identified in KABO crystals by electron paramagnetic resonance and optical absorption spectroscopy [10–12]. It is known [13] that ions of 3*d*-transition metals in strongly correlated compounds completely or partially determine their magnetic, optical, and other spectroscopic properties. The main reasons of this have to do with the strong electronic correlations and tight coupling between the spin, charge, and orbital degrees of freedom in the compounds of the 3*d* metals. In this connection, even the fairly low concentrations of impurity Fe^{3+} ions are responsible for intensive optical absorption bands in the UV region at 190–280 nm. This spectral region is very important for practical applications of KABO crystals, so considerable research efforts have been directed to the development of technology to reduce iron contamination in KABO crystals, for example by introducing impurity alkali ions of Na^+ [14–17] or the use of a reducing atmosphere in the growing process [18,19]. These efforts led to the successful growing of KABO crystals of high optical quality with relatively low iron contamination and thus with a fairly low UV optical absorption [18,19].

Luminescence spectroscopy method has high sensitivity and can significantly complement the optical spectroscopy data, especially at low concentration level of impurity Fe^{3+} ions. However, the luminescent properties of KABO crystals are poorly understood. We are aware of only few publications. Ogorodnikov et al. have determined the bandgap width of KABO crystals at 7 K as E_g = 8.0–8.5 eV; revealed and investigated the intrinsic luminescence of the host crystal at 3.28 eV, which is due to radiative annihilation of self-trapped excitons in KABO as well as they found the luminescence of defects at 2.68 and 3.54 eV [20,21]. The broadband red emission in KABO crystals at 1.65–1.75 eV has been observed and tentatively assigned to the $^4T_1(^4G) \rightarrow {}^6A_1(^6S)$ intracenter transitions in impurity Fe^{3+} ions

* Corresponding author. Tel.: +7 343 3754711; fax: +7 343 3743884.
E-mail address: i.n.ogorodnikov@gmail.com (I.N. Ogorodnikov).

0925-3467/$ - see front matter © 2013 Elsevier B.V. All rights reserved.
http://dx.doi.org/10.1016/j.optmat.2013.01.009

[12,20,21]. However, we are not aware of other research works on the red luminescence in KABO crystals.

The aim of this work is a spectroscopic study of the red-light-emitting centers in KABO:Fe, which are responsible for the red luminescence. Two spectroscopic methods were used in the research work: a low-temperature (7–293 K) luminescence spectroscopy upon selective photoexcitation by synchrotron radiation and optical absorption spectroscopy.

2. Experimental details

The examined $K_2Al_2B_2O_7$ crystals of high optical quality were grown at the Institute of Geology and Mineralogy SB RAS (Novosibirsk, Russia) using the flux method with top seed position. KABO crystal was grown on a seed oriented along the (1 1 0) direction at an initial temperature of 920 °C, thereafter the temperature was decreased with a rate of 2–4 °C a day. This provided a transparent hexagonal plates of 20 mm and a thickness of 1.5 mm. Other details of the growth process and crystal identification can be found in our previous works [20–22]. The samples for spectroscopic studies were prepared in the form of plane-parallel transparent plate of $6 \times 5 \times 1$ mm^3 size. The concentration of the impurity Fe^{3+} ions was chosen in the range of several few ppm to make its luminescence comparable in intensity with the other emission bands found previously in KABO crystals [21].

The present study was carried out by the means of the low-temperature luminescence VUV spectroscopy. The photoluminescence (PL) spectra in the energy range of E_m from 1.2 eV to 6.2 eV and the PL excitation (PLE) spectra in the energy range of E_{ex} from 3.7 eV to 21 eV (spectral resolution 0.32 nm) were recorded in the temperature range of 7–293 K at the SUPERLUMI experimental station of HASYLAB (DESY, Germany) [23] upon excitation with synchrotron radiation. At the storage ring DORIS the full width at half maximum (FWHM) of synchrotron radiation pulses was 130 ps with the repetition period of 96 ns. Samples were mounted in a sample holder attached to a He-flow cryostat with vacuum not less than 7×10^{-10} Torr. The primary 2 m-vacuum monochromator, equipped with Al-grating was used for selective PL excitation with synchrotron radiation. The PL excitation spectra were corrected to an equal number of photons incident on the sample using sodium salicylate. The 0.3 m ARC Spectra Pro-300i monochromator equipped with a cooled CCD-camera were used as a registration system. The PL emission spectra were not corrected to the spectral sensitivity of the recording system.

The UV–Vis optical absorption spectra were recorded at the laboratory of Solid State Physics of Ural Federal University (Yekaterinburg, Russia) by the means of the Helios Alpha UV–Vis spectrophotometer equipped with a Vision32 software.

3. Experimental results

Fig. 1a shows the optical absorption spectrum of KABO crystal recorded at room temperature. In the near-infrared and visible spectral regions, there is only a slight optical absorption. In the energy range from 3 to 7 eV there are four broad absorption bands at 3.6, 4.7 (I), 5.7 (II) and 6.5 eV (III) with the ratio of their intensities of 1:7:100:90. Three of the most intense absorption bands are indicated with Roman numerals I–III and shown in Fig. 1. The dominant absorption band at 5.7 eV is of 7.5 cm^{-1} in amplitude. Monotonic exponential increase of the optical absorption (Fig. 1), corresponding to the fundamental absorption edge of KABO crystal, is observed in the energy region above 6.8 eV.

Optical stimulation in these absorption bands provides efficient PL excitation in KABO. In this paper, we will focus on the study of low-temperature red luminescence of KABO crystals. The KABO

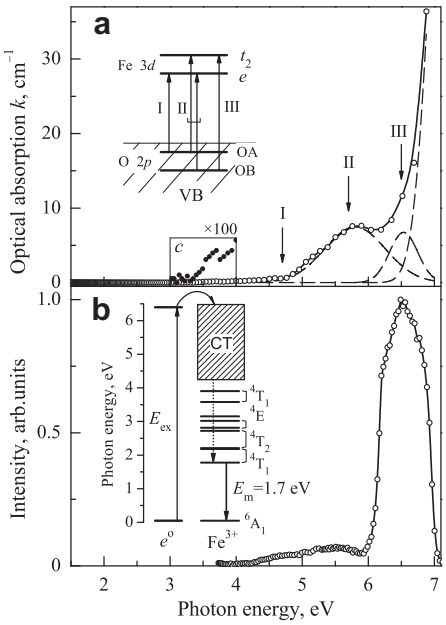

Fig. 1. Optical absorption spectrum (a) and PL excitation spectrum recorded monitoring emission at E_m = 1.7 eV (b) for KABO crystals at 293 (a) and 7 K (b). Panel (c) shows an enlarged fragment of the spectrum in the vicinity of the 3.6-eV absorption band. The insets show schematic energy diagrams illustrating (a) the charge transfer transitions that contribute to the optical absorption bands I–III and (b) energy transfer processes involved in deep-red luminescence upon excitation in the energy region of the fundamental absorption edge. CT denotes the energy range corresponding to the charge-transfer transitions; e^0 represents a free exciton in KABO.

Luminescence in the energy range of 2–5 eV has been previously studied in detail [21]. Fig. 1b shows PLE spectrum recorded for KABO crystal at 7 K monitoring emission at 1.7 eV. Energy positions of bands in PLE spectrum are coincident with those for the optical absorption spectrum, Fig. 1, but the ratio of their intensities are quite different. The 6.5 eV band dominates in PLE spectrum recorded monitoring emission at 1.7 eV, and all the other PLE bands are one order of magnitude lower in intensity. The high-energy slope of the 6.5 eV band is antibate to an increase of the optical absorption coefficient at the fundamental absorption edge of KABO crystal. In the energy range of the host absorption, PLE efficiency is negligible.

Fig. 2 shows PL emission spectra in the energy range of 1.4–2.0 eV recorded using CCD-camera for KABO crystal at various temperatures ranging from 7 to 80 K upon photoexcitation at E_{ex} = 6.78 eV. An intensive red PL emission band (*R*-band) with maximum at E_m = 1.675 eV (FWHM = 0.173 eV) is observed at 7 K. It should be noted that this value is a bit different from E_m = 1.72 eV, recorded earlier by means of a photomultiplier tube [20,21]. This is due to differences in the spectral sensitivity of the photomultiplier tube and the CCD-camera in this spectral region. The *R*-band is asymmetric in profile and has a more extended low-energy slope. Its formal approximation requires a minimum of two Gaussians with the intercenter distance of about 80 meV. However, an accurate analysis of the *R*-band shape is quite problematic, because the band is located fairly close to the low energy limit of operating spectral range of the recording system. An increase in temperature from 7 to 80 K causes a smooth decrease in the *R*-band intensity. For a correct measurement of the PL intensity above 40 K, we have considered the contribution of the low-energy tail from the PL emission bands located above 2.0 eV in the visible and near-UV spectral region. This contribution is shown by the dashed line in Fig. 2.

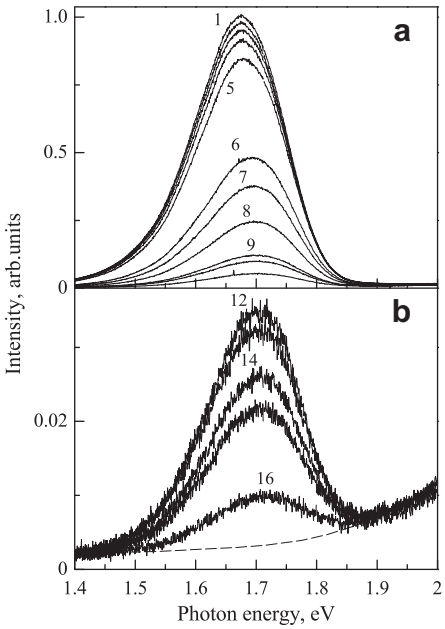

Fig. 2. PL emission spectra in the energy range of 1.4–2.0 eV recorded using CCD-camera upon photoexcitation at E_{ex} = 6.78 eV for KABO crystal at temperatures (a) 7 – (1), 8 – (2), 11.5 – (3), 14 – (4), 16.5 – (5), 25 – (6), 28.5 – (7), 32.5 – (8), 39.5 – (9), 41.5 – (10), 49 K – (11) and (b) 54.5 – (12), 55.5 – (13), 59 – (14), 62 – (15), 80.5 K – (16). The dashed line shows the contribution of PL emission bands located above 2.0 eV in the visible and near-UV spectral region.

In the temperature range from 15 to 25 K, the *R*-band is subject to a 20 meV-blue shift, while the bandwidth increases by about 10 meV, Fig. 3.

Fig. 4 shows the temperature dependence of the PL emission intensity recorded for KABO crystals monitoring emission at *R*-band upon excitation at E_{ex} = 6.78 eV. The experimental data are designated by open circles. For fitting the experimental data we used the sum of the two temperature quenching processes

$$I(T) = \sum_{i=1}^{2} \frac{I_i}{1 + \omega_i \exp(-E_i/k_B T)}, \quad (1)$$

here the best fit parameters are as follows: I_1 = 0.650 and I_2 = 0.345 are the low-temperature PL emission intensities before the temperature quenching started; E_1 = 9 and E_2 = 20 are the activation energies (meV); ω_1 = 220 and ω_2 = 1790 are dimensionless pre-exponential factors; k_B is the Boltzmann constant (eV/K); T is temperature (K).

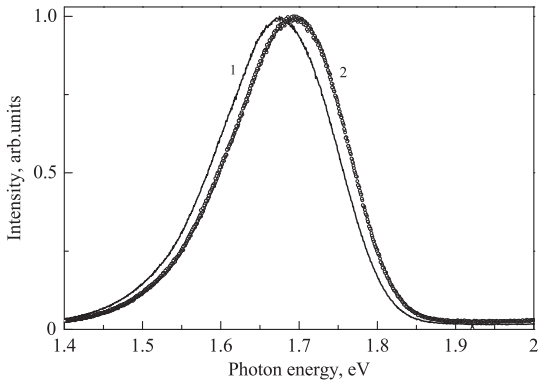

Fig. 3. Normalized PL emission spectra in the energy range of 1.4–2.0 eV recorded using CCD-camera upon photoexcitation at E_{ex} = 6.78 eV for KABO crystal at temperatures 7 – (1) and 25 K – (2).

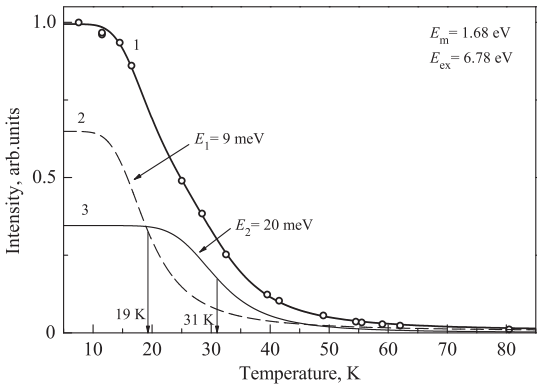

Fig. 4. Temperature dependence of the PL emission intensity recorded for KABO crystals monitoring emission at *R*-band upon excitation at E_{ex} = 6.78 eV. The experimental data are designated by open circles, smooth curve is the result of approximation – (1), and the elementary components of the PL temperature quenching – (2,3).

Vertical arrows in Fig. 4 denote the characteristic temperatures T_1 = 19 and T_2 = 31 K, at which the PL emission intensities of the first and second processes, are half their initial intensities. These data indicate that the first process (E_1 = 9 meV) has twice higher initial intensity, and it dominates in the temperature range from 7 to 15 K, while the second process (E_2 = 20 meV) dominates at 20–30 K. This explains the differences in the PL spectral composition at 7 and 25 K. Indeed, the low-energy PL emission band (Fig. 3) may be associated with the first process, while the 20 meV blue shifted PL band is due to the second process.

4. Discussion

The experimental results obtained in this study, as well as previously published data [10,11,20,21] indicate that KABO crystals contain minor concentrations of impurity Fe^{3+} ions, which, however, exert a significant influence on the optical and luminescent properties of KABO. This is favored by crystal-chemical features of KABO. Indeed, the crystallographic structure of $K_2Al_2B_2O_7$ contains a host Al^{3+} ions located in regular sites with tetrahedral coordination by oxygen ions. A regular tetrahedral site of host Al^{3+} ion is the most probable position for the impurity Fe^{3+} ion in KABO crystal (defect Fe_{Al}). Low defect creation energy of this center is due to equal charge states of the ions, and similar values of their radii (0.126 for Al^{3+} and 0.127 nm for Fe^{3+}). Electron paramagnetic resonance of KABO crystals indicated the presence of paramagnetic $Fe^{3+}O_4$ centers with a linear dependence of the g = 1.999 signal intensity on the concentration of iron impurity [10]. Let us discuss in more detail the possible optical and luminescence transitions in these centers.

4.1. Intraconfigurational d–d transitions in Fe^{3+} centers

A transition Fe^{3+} ion has the electron configuration [Ar] $3d^5$ with a partially filled outer shell of $3d^5$ electrons that are in the high-spin ground state and filling the sole spin sextet and orbital singlet $^6S_{5/2}$ [24]. Impurity Fe^{3+} cations in oxide crystals usually occupy positions of the O_h or T_d symmetry, with the octahedral or tetrahedral coordination by negative oxygen ions. Fe^{3+} ion has an equal probability to occupy any of these positions [25]. The results of calculations of the electronic energy structure of $[FeO_6]^{9-}$ and $[FeO_4]^{5-}$ clusters with Fe^{3+} ions in octahedral and tetrahedral sites surrounded by oxygen ions [26–33] showed that in the high-spin complexes of tetrahedral coordination, the lowest electron configuration $(e)^2$ $(t_2)^3$ of ^6S states of Fe^{3+} ion will generate the $^6A_1$ ground

state. The lowest excited state (^4G) of free iron ion in a tetrahedral crystal field will be split into $^4T_1$, $^4T_2$, and ^4E, $^4A_1$ levels [26]. Fig. 1b shows a schematic energy diagram of Fe^{3+} ion a tetrahedral crystal field. All the optical d–d transitions from the $^6A_1$ ground state onto the spin quartets and doublets are forbidden by spin and parity. In the spectral region of these transitions one can expect only a relatively weak optical absorption due to the partial removal of these prohibitions by various perturbations, such as distortion of the crystal field, the lattice vibrations, spin orbit coupling. This is quite consistent with our experimental data: the value of the optical absorption of KABO crystal at energies below 3 eV is extremely low, and in the energy range of 3–4.5 eV one can observe only the low-intensity broad bands of optical absorption, Fig. 1a. Intraconfigurational d–d transitions in KABO crystals can be observed only at a sufficiently higher concentration of impurity Fe^{3+} ions. For instance, Wang et al. observed d–d transitions in KABO crystals at a concentration of impurity Fe^{3+} ions of 6.3 at.% [12].

4.2. Optical transitions with charge transfer O–Fe

The intensive optical absorption bands at 4.7, 5.7 and 6.5 eV (Fig. 1a) should be attributed to electric dipole allowed optical transitions with charge transfer O–Fe. Similar transitions have been previously found in many crystals containing transition ions [24,26,28]. However, the detailed theoretical interpretation of these transitions has been made only for certain crystals, and in most cases they used the cubic symmetry approximation. Lin et al. performed first-principles electronic structure calculations of KABO crystals with impurity Fe^{3+} ions [11]. The results [11] shows that the upper part of the valence band (VB) of KABO, which is located below the VB top in the energy range from −4 to 0 eV, is due to O 2p orbitals, whereas K 4s orbitals contribute to the conduction band bottom. Substitution of host Al^{3+} ion by iron impurity leads to the creation of a number of local states. Two peaks of the local density of states in the bandgap of the crystal at 4 and 5 eV above the VB top, are induced by the vacant Fe 3d 'spin-down' orbitals. Filled Fe 3d 'spin-up' orbitals and local O^{2-} 2p levels are located in VB of KABO crystal. In this case, the O^{2-} 2p 'spin-down' levels are located below the VB top at −0.3 and −1.3 eV [11]. These energy levels are shown in Fig. 1 as the OA and OB levels, respectively. From the crystal field theory, this result can be interpreted as follows. Tetrahedral symmetry crystal field splits the fivefold degenerate ^6S level of $3d^5$ electrons of Fe^{3+} ion, into two energy levels. Doubly degenerate lower level (e) and triply degenerate upper level (t_2), separated by the $10Dq$ energy gap, form a 'spin-up' electronic configuration $(e)^{2\uparrow}(t_2)^{3\uparrow}$ with an effective spin of 5/2. All the 'spin-down' configurations of Fe 3d orbitals are vacant, and completely filled O^{2-} 2p orbitals correspond to the highest occupied states of $[FeO_4]^{5-}$. If the photon energy is sufficient, we will observe the optical absorption due to the electron transitions from the 'spin-down' O^{2-} 2p states labeled as OA and OB (Fig. 1), onto the vacant 3d states of Fe^{3+} ions located in the crystal bandgap.

These data allow us to interpret the most intensive optical absorption bands at 4.7, 5.7 and 6.5 eV (Fig. 1a) in the following manner. Two electronic transitions occur from O^{2-} 2p level (OA-level), which is located in VB at −0.3 eV, onto the vacant e and t_2 orbitals of impurity Fe^{3+} ions, which are located in the crystal bandgap. Optical transition $\rightarrow e$ causes the 4.7 eV band, and the transition OA $\rightarrow t_2$ contributes to the 5.7 eV band.

The difference between the energy positions of the maxima of the charge transfer absorption bands can be an estimate of the energy gap of $10Dq \approx 5.7 - 4.7 = 1$ eV. The resulting value of $10Dq$ is consistent with the known data on aluminates of alkali metals with tetrahedral coordination of the impurity Fe^{3+} ions, such as 0.99 eV in $LiAl_5O_8$ [34], 1.2 eV in orthoclase [35], as well as with the calculated data obtained by the SSF-X_α – SW method for the electronic structure of $[FeO_4]^{5-}$ cluster [27].

Another two electronic transitions occur from O^{2-} 2p level (OB-level), which is located in VB at −1.3 eV, onto the vacant e and t_2 orbitals of impurity Fe^{3+} ion, which are located in the crystal bandgap. Transition OB $\rightarrow e$ should contribute to the low-energy slope of the 5.7 eV band, but this contribution was not recognized by the decomposition of the absorption spectrum in Fig. 1a. Another transition OB $\rightarrow t_2$ causes the optical absorption band at 6.5 eV.

The concentration of impurity Fe^{3+} ions in KABO crystal determines the intensity of the optical absorption bands. The calibration coefficient for the 4.7 eV absorption band is $\alpha = 0.27\ cm^{-1}$/ppm [10]. Applying this factor to our data (Fig. 1a), we found the concentration of Fe^{3+} ions in the KABO crystals is approximately 2 ppm. This looks quite plausible, since it is known [36], the concentration of iron impurity in several few ppm may cause the observed UV absorption in many compounds.

4.3. Luminescence of impurity Fe^{3+} ions

Low-temperature red luminescence in KABO crystals containing impurity Fe^{3+} ions (Fig. 2), manifests itself at 1.675 eV (FWHM = 0.173 eV), and its properties correspond to intracenter emissions caused by radiative transitions $^4T_1(G) \rightarrow {}^6A_1(S)$ in the impurity Fe^{3+} ion located in a tetrahedral site. Let us discuss this in more detail.

Luminescence of Fe^{3+} ions in the deep-red spectral region was found in many optical materials and natural minerals, such as $Li(Ga,Al)_5O_8$ [37–40], (Sc, Lu, Y) PO_4 [41], feldspars various compositions [35,42,43], PLZT-ceramics [44], α–Ga_2O_3[45], γ-AlF_3 [46], ZnO [47] and Zn_2SiO_4 [48]. These studies have identified three important facts. First, in all cases, the deep-red PL emission band is due intracenter radiative transitions in Fe^{3+} ions from the lowest excited $^4T_1(G)$ state onto the ground $^6A_1(S)$ state. Second, the energy position of this PL emission band depends on the coordination of Fe^{3+} ions: in the case of tetrahedral coordination, the band maximum is observed in the red spectral region at 1.65–1.98 eV, and in the case of octahedral coordination, the band maximum is located in the near-infrared spectral region at 1.36–1.48 eV. Third, in most cases, even at very low temperatures, the PL emission band has a Gaussian shape with a FWHM of 0.18–0.37 eV [49]. The fine structure of the PL emission spectrum can be observed only in certain compounds. For example, a narrow zero-phonon line and the vibrational structure of the PL emission spectrum at 1.65–1.90 eV can be observed at 4.2 K in the ordered phase of $LiAl_5O_8$:Fe^{3+} crystals [34,37,50,51].

The repetition period of the excitation pulses of synchrotron radiation in our measurements was 96 ns. In this regard, the PL decay kinetics recorded monitoring emission at 1.675 eV looked like a constant level – a pedestal, which corresponded to the total contribution from the slow components of the micro- and millisecond decay-time range. Such slow PL decay kinetics indicates the prohibited nature of radiative transitions and provides indirect evidence for its connection with the d–d transitions in Fe^{3+} ions. This is quite consistent with published data on other matrices containing Fe^{3+} ions: the time constant of the PL decay kinetics at 1.65–1.98 eV is 25.2 ms in ZnO:Fe^{3+} crystals [47], a few milliseconds in hydrated volcanic glasses doped with Fe^{3+} ions [52], 1.72–6.20 ms in $LiAl_5O_8$:Fe^{3+} [53].

PLE spectrum of R-band and optical absorption spectrum (Fig. 1) are comparable on a set of observed peaks, the highest PLE-efficiency is observed in the energy range of I–III optical absorption bands corresponding to the charge transfer transitions. Such a correspondence between the PLE-spectrum of R-band and optical absorption spectrum is typical of many matrices containing Fe^{3+} ions. For example, PLE-spectra of R-band in aluminate and alkali

metal phosphates showed weak bands of *d–d* transitions in Fe^{3+} ions and dominant bands corresponding to the charge transfer optical transitions [34,39,41]. However, the 6.5 eV dominant band in the PLE-spectrum of *R*-band (Fig. 1b) exceeds all other PLE-bands in intensity by more than one order of magnitude, whereas the II and III bands in the optical absorption spectrum (Fig. 1a) are approximately equal in intensity.

In our opinion, the direct photoexcitation of the charge-transfer transitions O–Fe occurs in the energy region from ca. 4.5 to 7 eV. This corresponds to a relatively moderate luminescence intensity upon excitation in the energy range of the I and II bands (Fig. 1b). In addition to this mechanism, in the energy region of 6–7 eV there is an excitonic channel for the energy transfer from the matrix to the impurity Fe^{3+} ions. This leads to a substantial increase of PL intensity upon excitation in the energy range of the III band. Fig. 1b shows a schematic diagram illustrating the energy transfer processes involved in deep-red luminescence upon excitation in the energy region of the fundamental absorption edge. The following arguments are evidence in favor of this assertion. The energy range of 6–7 eV corresponds to the fundamental absorption edge of KABO crystal. Ogorodnikov et al. have revealed the direct photoexcitation of the mobile excitons in this energy range [20]. PLE-spectrum recorded monitoring emission of self-trapped excitons in KABO shows the dominant peak at 6.84 eV (FWHM = 0.41 eV), but its low-energy slope extends down to energy of 6 eV [21]. The 6.5 eV band is observed in both the PLE and optical absorption spectra (Fig. 1), and the values of its FWHM in these spectra are quite similar (0.78 and 0.65 eV, respectively). In addition, there is a coincidence of high-energy slopes of the excitation bands of both the *R*-luminescence (Fig. 1b) and luminescence of self-trapped excitons [21]. A similar excitation mechanism has been previously found in certain other oxide crystals, e.g. in beryllium oxide [54] and lithium triborate [55].

It should be noted that the possible contribution from the impurity-bound excitons into the *R*-luminescence excitation is not considered here, since the probability of their excitation is negligible due to the low concentration of impurity Fe^{3+} ions (ca. 2 ppm). Moreover, the relatively large band width (0.78 eV) of the 6.5 eV PLE band (Fig. 1b) also indicates not in favor of the impurity-bound excitons.

4.4. Temperature dependence of the red luminescence intensity

The 20 meV blue-shift of the PL emission band in the temperature range from 15 to 25 K and its broadening by 10 meV indicate, in our view, the manifestation of two different types of red-light-emitting centers, causing the two different bands of *R*-luminescence, Fig. 3. Indeed, *R*-luminescence in KABO crystals is due to the radiative ${}^6A_1(S) \rightarrow {}^4T_1(G)$ transitions. According to the Tanabe–Sugano diagram for Fe^{3+} ion in tetrahedral coordination [27], these transitions are strongly dependent on the crystal field, so that small changes in the field will significantly affect both the energy position and band-width of the PL emission band. Energy position of the first excited level of ${}^4T_1(G)$ in the cluster $[FeO_4]^{5-}$ determined by the strength of the ligand field $10Dq$ and Racah parameters B and C: a decrease of $10Dq/B$ leads to a shift in position of ${}^4T_1(G)$ level to higher energies, causing a blue shift of the PL emission band. Crystal-field parameters depend on the length and covalency of Fe–O bonds, which, in turn, is subject to the influence of the elemental composition of the nearest environment [42,43,46,49], the distribution of Al^{3+} cations between nonequivalent positions [39,56], the creation of lattice defects, compensating the impurity excess charge or the difference in the ionic radii [39,48].

The most likely reason for the change in Fe–O bonds, in our view, is the existence two non-equivalent regular positions of KABO crystal lattice occupied by Al^{3+} ions. The concentration ratio

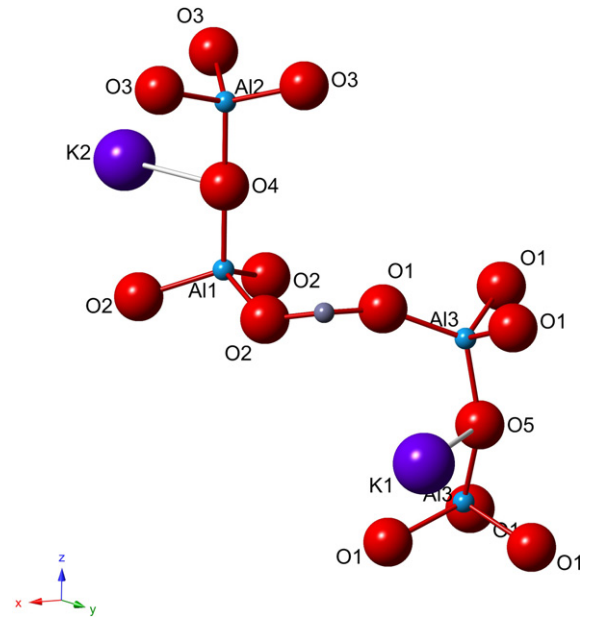

Fig. 5. Fragment of KABO crystallographic structure containing two nonequivalent Al_2O_7 clusters.

of these non-equivalent positions in KABO crystal is 2:1 [3]. Assuming that the impurity Fe^{3+} ions can occupy with equal probability any of these positions of KABO lattice, we should expect the presence of two different impurity $Fe_{Al}{}^{3+}$ centers with concentration ratio of 2:1. Crystal-field parameters of these centers will also vary, resulting in two different bands of *R*-luminescence. Fig. 5 shows a fragment of the KABO crystallographic structure containing two nonequivalent Al_2O_7 clusters. For each cluster with $Al_3–O_5–Al_3$ atoms there are two clusters with $Al_1–O_4–Al_2$ atoms [3]. The most intensive component (E_1 = 9 meV) of the temperature quenching (Fig. 4) dominates in the low-temperature PL emission band (Fig. 3). It should be associated with the impurity Fe^{3+} ion, which has replaced Al^{3+} ion in $Al_1–O_4–Al_2$ cluster. The second component (E_1 = 20 meV) of the temperature quenching (Fig. 4) dominates above 20 K and determines the PL emission spectrum at 25 K (Fig. 3). It should be attributed to the impurity Fe^{3+} ion, which has replaced Al^{3+} ion in $Al_3–O_5–Al_3$ cluster. The activation energies of thermal quenching (9 and 20 meV) fall into the phonon energy band of KABO at 8–45 meV (69–360 cm^{-1}), which is caused by the external vibrations originating from the translational motions of K ion and anion group plus the librational motion of the anion group [57]. In this connection, the thermal quenching of *R*-luminescence can be attributed to the electron–phonon interaction in the appropriate Al_2O_7 cluster.

5. Conclusions

Thus, we have investigated the low-temperature red-light-emitting centers in $K_2Al_2B_2O_7:Fe^{3+}$ using the methods of optical absorption spectroscopy and low-temperature luminescence spectroscopy with selective excitation by synchrotron radiation. It was found that the luminescence at 1.675 eV (FWHM = 0.173 eV) is due to the intracenter ${}^4T_1({}^4G) \rightarrow {}^6A_1({}^6S)$ transitions in impurity Fe^{3+} ions. At 7 K it is efficiently excited in the excited region at the fundamental absorption edge of KABO crystal. An elevated excitation efficiency is due to partial overlapping of the fundamental absorption edge of the crystal, where the excitation of mobile excitons occurs, and the broad absorption band of the charge transfer O–Fe with a maximum at 6.5 eV. It is shown that the observed spectrum

of the luminescence is due to the superposition of two Fe^{3+} luminescence centers with the ratio of their contributions of 2:1. The temperature dependence of the luminescence is a superposition of the processes of thermal quenching of these centers with activation energies of 9 and 20 meV, respectively. The nature of the red-light-emitting centers can be associated with the presence of two non-equivalent regular Al^{3+} positions of KABO lattice, which are located in two non-equivalent Al_2O_7 clusters with a concentration ratio of 2:1. Thermal quenching of *R*-luminescence, in our opinion, can be attributed to the electron–phonon interaction in the appropriate cluster Al_2O_7.

The observed phenomenon of high energy excitation, leading to photon yield in the red, where 3/4 of the energy is lost into the lattice, is very important for practical applications of KABO crystals. Indeed, the broad band at 6.5 eV is located in the energy region of the fourth harmonic of the laser with a fundamental wavelength of 1064 nm. Energy dissipation mechanism identified in this paper, explains why such a low concentration of the iron impurity ions (ca. 2 ppm) so strongly affect the optical properties of KABO at the low energy tail of the host absorption.

Full spectroscopic characterization of these red-light-emitting centers also requires polarization measurements for the absorption and luminescence spectra, as it was done previously for some other optical crystals, such as BeO [58] and LiB_3O_5 [59]. However, the absence of oriented crystals, large in all three crystallographic directions, does not allow yet to perform such measurements for KABO.

Acknowledgments

The authors are very grateful to S.A. Zhurkov for his help in preparing the crystals examined. The work was partially supported by HASYLAB DESY (Project No. 20110843), and the Siberian Branch of the Russian Academy of Sciences (Grant No. 28).

References

[1] N. Ye, W. Zeng, B. Wu, Ch. Chen, Proc. SPIE 3556 (1998) 21–23.
[2] Z.G. Hu, Y. Mori, T. Higashiyama, M. Yoshimura, Y.K. Yap, Y. Kagebayash, T. Sasaki, Proc. SPIE 3556 (1998) 156–161.
[3] J.A. Kaduk, L.C. Satek, S.T. Mckenna, Rigaku J. 16 (2) (1999) 17–30.
[4] Ch. Chen, Laser Focus World 40 (2) (2004) 91–95.
[5] N. Ye, W. Zeng, J. Jiang, B. Wu, Ch. Chen, B. Feng, X. Zhang, J. Opt. Soc. Am. B-Opt. Phys. 17 (2000) 764–768.
[6] J. Lu, G. Wang, Z. Xu, Ch. Chen, J. Wang, C. Zhang, Y. Liu, Chin. Phys. Lett. 19 (2002) 680–681.
[7] P. Kumbhakar, S. Adachi, Z.-G. Hu, M. Yoshimura, Y. Mori, T. Sasaki, T. Kobayashi, Jpn. J. Appl. Phys. 42 (2003) L1255–L1258.
[8] N. Umemura, M. Ando, K. Suzuki, E. Takaoka, K. Kato, Z.-G. Hu, M. Yoshimura, Y. Mori, T. Sasaki, Appl. Opt. 42 (2003) 2716–2719.
[9] Z.G. Hu, T. Higashiyama, M. Yoshimura, Y. Mori, T. Sasaki, Z. Kristallogr, New Cryst. Struct. 214 (4) (1999) 433–434.
[10] L. Liu, C. Liu, X. Wang, Z.G. Hu, R.K. Li, Ch.T. Chen, Solid State Sci. 11 (4) (2009) 841–844.
[11] Z.S. Lin, L.F. Xu, L. Liu, J. Xu, M.H. Lee, Z. Fang, Ch.T. Chen, Phys. Rev. B: Condens. Matter 82 (2010) 035124. 6.
[12] Y. Wang, R.K. Li, Opt. Mater. 32 (10) (2010) 1313–1316.
[13] V.F. Agekyan, Phys. Solid State 44 (11) (2002) 2013–2030.
[14] C. Zhang, J. Wang, X. Cheng, X. Hu, H. Jiang, Y. Liu, Ch. Chen, Opt. Mater. 23 (1–2) (2003) 357–362.
[15] Y.G. Wang, R.K. Li, J. Synth. Cryst. 39 (Suppl.) (2010) 1–4.
[16] Y. Yue, Z. Wu, Z. Lin, Z. Hu, Solid State Sci. 13 (5) (2011) 1172–1175.
[17] Z. Wu, Y. Yue, L. Wang, G. Wang, Z. Hu, Opt. Mater. 34 (9) (2012) 1575–1578.
[18] Y. Wang, L. Wang, X. Gao, G. Wang, R.K. Li, Ch.T. Chen, J. Cryst. Growth 348 (1) (2012) 1–4.
[19] C. Liu, L. Liu, X. Zhang, L. Wang, G. Wang, Ch. Chen, J. Cryst. Growth 318 (1) (2011) 618–620.
[20] I.N. Ogorodnikov, V.A. Pustovarov, S.A. Yakovlev, L.I. Isaenko, S.A. Zhurkov, Phys. Solid State 54 (1) (2012) 111–116.
[21] I.N. Ogorodnikov, V.A. Pustovarov, S.A. Yakovlev, L.I. Isaenko, S.A. Zhurkov, J. Lumin. 132 (7) (2012) 1632–1638.
[22] L.I. Isaenko, A.P. Yelisseyev, Chem. Sust. Develop. 8 (2000) 213–217.
[23] G. Zimmerer, Radiat. Meas. 42 (4–5) (2007) 859–864.
[24] A.B.P. Lever, Inorganic Electronic Spectroscopy, Elsevier, Amsterdam, Oxford, New York, Tokio, 1985. 864 pp.
[25] R.M. Cornell, U. Schwertmann, The Iron Oxides: Structure, Properties, Reactions, Occurrences and Uses, Wiley-VCH Verlag GmbH & Co. KGaA, 2003. 703 pp.
[26] D.M. Sherman, T.D. Wait, Am. Mineral. 70 (11–12) (1985) 1262–1269.
[27] D.M. Sherman, Phys. Chem. Miner. 12 (3) (1985) 161–175.
[28] D.M. Sherman, Am. Mineral. 75 (3–4) (1990) 256–261.
[29] M. Lenglet, M. Bizi, C.K. Jørgensen, J. Solid State Chem. 86 (1) (1990) 82–87.
[30] V.V. Alekseev, V.V. Druzhinin, R.V. Pisarev, Sov. Phys. Solid State 33 (9) (1991) 1507–1510.
[31] V.V. Pavlov, R.V. Pisarev, M. Fiebig, D. Fröhlich, Phys. Solid State 45 (4) (2003) 662–669.
[32] P.A. Usachev, R.V. Pisarev, A.M. Balbashov, A.V. Kimel, A. Kirilyuk, T. Rasing, Phys. Solid State 47 (12) (2005) 2292–2298.
[33] V.V. Pavlov, A.R. Akbashev, A.M. Kalashnikova, V.A. Rusakov, A.R. Kaul, M. Bayer, R.V. Pisarev, J. Appl. Phys. 111 (5) (2012) 056105.
[34] G.T. Pott, B.D. McNicol, J. Chem. Phys. 56 (11) (1972) 5246–5254.
[35] W.B. White, M. Matsumura, D.G. Linnehan, T. Furukawa, B.K. Chandrasekhar, Am. Mineral. 71 (1986) 1415–1419.
[36] H.H. Tippins, Phys. Rev. B: Condens. Matter 1 (1970) 126–135.
[37] N.T. Melamed, J.M. Neto, T. Abritta, F. de Souza Barros, J. Lumin. 24–25 (Part 1) (1981) 249–252.
[38] J.M. Neto, T. Abritta, F. de Souza Barros, N.T. Melamed, J. Lumin. 22 (2) (1981) 109–120.
[39] T.R.N. Kutty, M. Nayak, J. Alloys Compd. 269 (1–2) (1998) 75–78.
[40] A.P. Jadhav, A. Pawar, U. Pal, B.K. Kim, Y.S. Kang, Sci. Adv. Mater. 4 (2012) 597–603.
[41] E.W.J.L. Oomen, K. van der Vlist, W.M.A. Smit, G. Blasse, Chem. Phys. Lett. 129 (1) (1986) 9–12.
[42] M.R. Krbetschek, J. Götze, G. Irmer, U. Rieser, T. Trautmann, Mineral. Petrol. 76 (2002) 167–177.
[43] R.J. Brooks, A.A. Finch, D.E. Hole, P.D. Townsend, Z.-L. Wu, Contrib. Mineral. Petrol. 143 (2002) 484–494.
[44] S. Murakami, M. Herren, D. Rau, M. Morita, Inorg. Chim. Acta 300–302 (2000) 1014–1021.
[45] G.T. Pott, B.D. McNicol, J. Lumin. 6 (3) (1973) 225–228.
[46] D.J. Telfer, G. Walker, J. Lumin. 11 (5–6) (1976) 315–320.
[47] R. Heitz, A. Hoffmann, I. Broser, Phys. Rev. B: Condens. Matter 45 (16) (1992) 8977–8988.
[48] E. Cavalli, A. Belletti, E. Zannoni, J. Solid State Chem. 117 (1) (1995) 16–20.
[49] P.A. Bingham, J.M. Parker, T.M. Searle, I. Smith, J. Non-Cryst. Solids 353 (2007) 2479–2494.
[50] N.T. Melamed, F. de Souza Barros, P.J. Viccaro, J.O. Artman, Phys. Rev. B: Condens. Matter 5 (1972) 3377–3387.
[51] T. Abritta, F. de Souza Barros, N.T. Melamed, J. Lumin. 33 (2) (1985) 141–146.
[52] N. Zotov, Y. Yanev, B. Piriou, Phys. Chem. Miner. 29 (2002) 291–299.
[53] N.T. Melamed, P.J. Viccaro, J.O. Artman, F. de Souza Barros, J. Lumin. 1–2 (1970) 348–367.
[54] I.N. Ogorodnikov, V.Yu. Ivanov, A.V. Kruzhalov, Radiat. Meas. 24 (4) (1995) 417–421.
[55] I.N. Ogorodnikov, A.V. Kruzhalov, E.A. Radzhabov, L.I. Isaenko, Phys. Solid State 41 (2) (1999) 197–201.
[56] W. Shu, R.F. Qiang, S. Xiao, X. Yang, J.W. Ding, J. Alloys Compd. 509 (2011) 3886–3888.
[57] X.B. Hu, J.Y. Wang, C.Q. Zhang, X.G. Xu, C.-K. Loong, M. Grimsditch, Appl. Phys. Lett. 85 (12) (2004) 2241–2243.
[58] V.Yu. Ivanov, V.A. Pustovarov, A.V. Korotaev, A.V. Kruzhalov, M. Kirm, G. Zimmerer, Surf. Rev. Lett. 9 (2) (2002) 1291–1295.
[59] I.N. Ogorodnikov, V.A. Pustovarov, A.V. Porotnikov, A.V. Kruzhalov, Nucl. Instrum. Methods Phys. Res. A405 (2–3) (1998) 403–407.